Journal of Translational Medicine

RESEARCH

Open Access

# Hsa_circ_0002301 inhibits ferroptosis in gastric cancer by encoding the de novo protein HECTD1-463aa

Song Wang[1,3†], Chengwei Wu[1,3†], Jiawei Wang[1,3†], Feng Yuan[4†], Yinfen Hou[5], Tingting Cao[1,3], Lishuai Xu[1,3], Long Qian[1,3], Yabin Xia[1,3], Li Xu[1,3], Ailiang Zeng[6], Xiaoming Wang[7], Luman Wang[2*] and Xiaoxu Huang[1,3*]

## Abstract

**Background** CircRNAs are closely related to ferroptosis in gastric cancer cells; however, the mechanism by which circRNAs regulate ferroptosis in gastric carcinogenesis remains unknown. CircRNA-encoded novel peptides are functional products translated from the open reading frames (ORFs) within circular RNAs, demonstrating that circRNAs not only serve as non-coding regulators but also have the capacity to encode biologically active peptides. Compared with noncancerous cells, cancer cells have greater iron requirements, and ferroptosis occurs in response to radiotherapy, chemotherapy, and immunotherapy; therefore, ferroptosis activation may be a potential strategy to overcome the shortcomings of conventional cancer therapy.

**Methods** A mouse model of ferroptosis in gastric cancer was constructed, and a bioinformatics analysis was performed to analyze and characterize the circRNAs involved in ferroptosis in gastric cancer. The inhibitory effect of hsa_circ_0002301 on ferroptosis in tumors was confirmed both in vitro and in vivo. The presence and expression of HECTD1-463aa were verified using mass spectrometry, protein blotting, and immunofluorescence staining. The molecular mechanism of hsa_circ_0002301 was investigated using mass spectrometry and immunoprecipitation.

**Results** We designed and synthesized antibodies specific for the small protein HECTD1-463aa encoded by hsa_circ_0002301 to verify its presence and purified HECTD1-463aa by constructing hsa_circ_0002301 overexpression vectors with FLAG tags and used liquid chromatography–tandem mass spectrometry (LC–MS/MS) to detect the characterized peptides. In addition, HECTD1 binding to HECTD1-463aa was identified by immunoprecipitation (Co-IP) and mass spectrometry. We found that HECTD1-463aa inhibited HECTD1-mediated GPX4 ubiquitination by binding to HECTD1, an important regulator of cell death in ferroptotic cancer cells.

**Conclusions** hsa_circ_0002301 competitively inhibits the degradation of the GPX4 protein by HECTD1 through the encoded proteins HECTD1-463aa and HECTD1 to affect the ferroptosis level in gastric cancer cells.

†Song Wang, Chengwei Wu, Jiawei Wang and Feng Yuan have contributed equally to this work.

*Correspondence:
Luman Wang
lumanwang@fudan.edu.cn
Xiaoxu Huang
xiaoxuhuang1984@163.com

Full list of author information is available at the end of the article

## Background

Gastric cancer (GC), the fifth most prevalent malignancy worldwide, accounts for more than a million new diagnoses annually and is the third leading cause of cancer-related mortality globally [1, 2]. Gastric cancer is often diagnosed at an advanced stage and is the third leading cause of cancer-related death. In 2018 alone, 784,000 individuals worldwide died from this disease [3, 4]. Hence, substantial gaps and formidable challenges exist in gastric cancer treatment. In 2012, Dixon introduced the concept of ferroptosis [5], a distinct form of non-apoptotic cell death triggered by lipid peroxidation [6, 7]. Owing to their physiological differences in iron and lipid metabolism, along with the abnormal production of reactive oxygen species (ROS) [8, 9], cancer cells may be more susceptible to the regulation of ferroptosis than normal cells [10, 11]. Regardless of whether ferroptosis is a physiological process of normal cell death or a pathological anomaly, the development of a drug that can induce ferroptosis in cancer cells while sparing normal cells could provide substantial benefits in cancer treatment [12, 13]. An increasing number of anticancer drugs have been shown to trigger ferroptosis. Cancer cells require a greater amount of iron to fuel their growth than noncancerous cells. Ferroptosis can be observed in response to radiotherapy, chemotherapy, and tumor immunotherapy. The activation of ferroptosis may be a strategy for overcoming the limitations of traditional cancer treatments [14, 15].

Recent research has revealed a close relationship between noncoding RNAs (ncRNAs) and ferroptosis in gastric cancer cells [16, 17]. A growing body of evidence suggests that circular RNAs (circRNAs) containing internal ribosome entry sites (IRESs) or extensive N6-methyladenosine (m6A) sites can regulate the progression of gastric cancer by encoding proteins [18, 19], in contrast to the conventional definition of ncRNAs. Many studies have identified numerous circRNA-encoded proteins that are closely related to tumors. The up- or downregulation of these circRNA-encoded proteins, the activation of corresponding downstream signaling pathways, or the modification of specific molecules affects the epigenetic function of tumor cells or their resistance to chemotherapy in a variety of ways, ultimately mediating tumorigenesis and tumor progression [20]. Peptides encoded by circular RNAs have biological functions in the occurrence and progression of diseases such as cancer. For example, some peptides encoded by circular RNAs can inhibit tumor angiogenesis, thus playing an anticancer role [21]. These peptides may also be used as biomarkers of cancer prognosis and as targets of antitumor drugs [21, 22]. However, whether circRNAs regulate ferroptosis by encoding proteins, thereby affecting the initiation and progression of gastric cancer, remains unclear. CircRNAs are important regulatory factors in the development of GC, and further exploration of their impacts on the pathogenesis of GC is crucial. These findings could pave the way for identifying novel diagnostic and therapeutic targets for gastric cancer [23, 24].

To date, some studies have suggested that inducing ferroptosis in cancer cells can impede tumor progression. Specific anticancer drugs can inhibit molecules and channels associated with iron metabolism, such as glutathione peroxidase 4 (GPX4) and system Xc-, thereby inducing ferroptosis in cancer cells and inhibiting tumor growth [25, 26]. However, most of these studies have focused primarily on gastric cancer cell lines, providing insights into the role of ferroptosis in the malignant transformation of tumor cells. No information has been reported on the impact of ferroptosis on tumor initiation and progression in vivo [27, 28]. Our research group previously established a C57BL/6 mouse model of gastric cancer induced by N-methyl-N-nitrosourea (MNU) and employed a ferroptosis inducer, piperazine erastin (PE), which is suitable for in vivo experiments, to induce ferroptosis in mice as a method to address this knowledge gap [29].

## Results

### Elevated hsa_circ_0002301 levels are correlated with ferroptosis in a gastric cancer model

We induced ferroptosis in a murine model of MNU-induced gastric cancer to investigate the impact of ferroptosis on the initiation and progression of gastric cancer and identified the differentially expressed circRNAs. After 40 weeks of treatment, peripheral blood was collected from the abdominal aorta, and the gastric tissue was harvested (Fig. 1a). Through the measurement of ROS levels, malondialdehyde(MDA) levels, $Fe^{2+}$ accumulation, and the glutathione (GSH)/oxidized glutathione (GSSG) ratio in gastric cancer tissues, we found that PE treatment induced significant increases in lipid ROS and MDA levels and $Fe^{2+}$ accumulation, accompanied by a decrease in the GSH/GSSG ratio, confirming the successful induction of ferroptosis in mice (Fig. 1b). Moreover, differences in the expression levels of classic ferroptosis negative regulatory (FNR) proteins were induced by PE. Interestingly, as the dose of PE injected into the mice increased, the expression of FNR proteins decreased significantly. Moreover, the expression of FNR proteins in the gastric cancer tissues of the mice was higher than that in the adjacent nontumor tissues (Fig. 1c; Fig. S6a). Compared with those in the control group, the sizes and weights of the tumors in the PE group were significantly smaller than those in the MNU group (Fig. 1d). Hematoxylin–eosin (H&E) staining revealed a more robust pathological morphology in gastric cancer tissues with a higher level of ferroptosis, and Ki-67 staining showed a

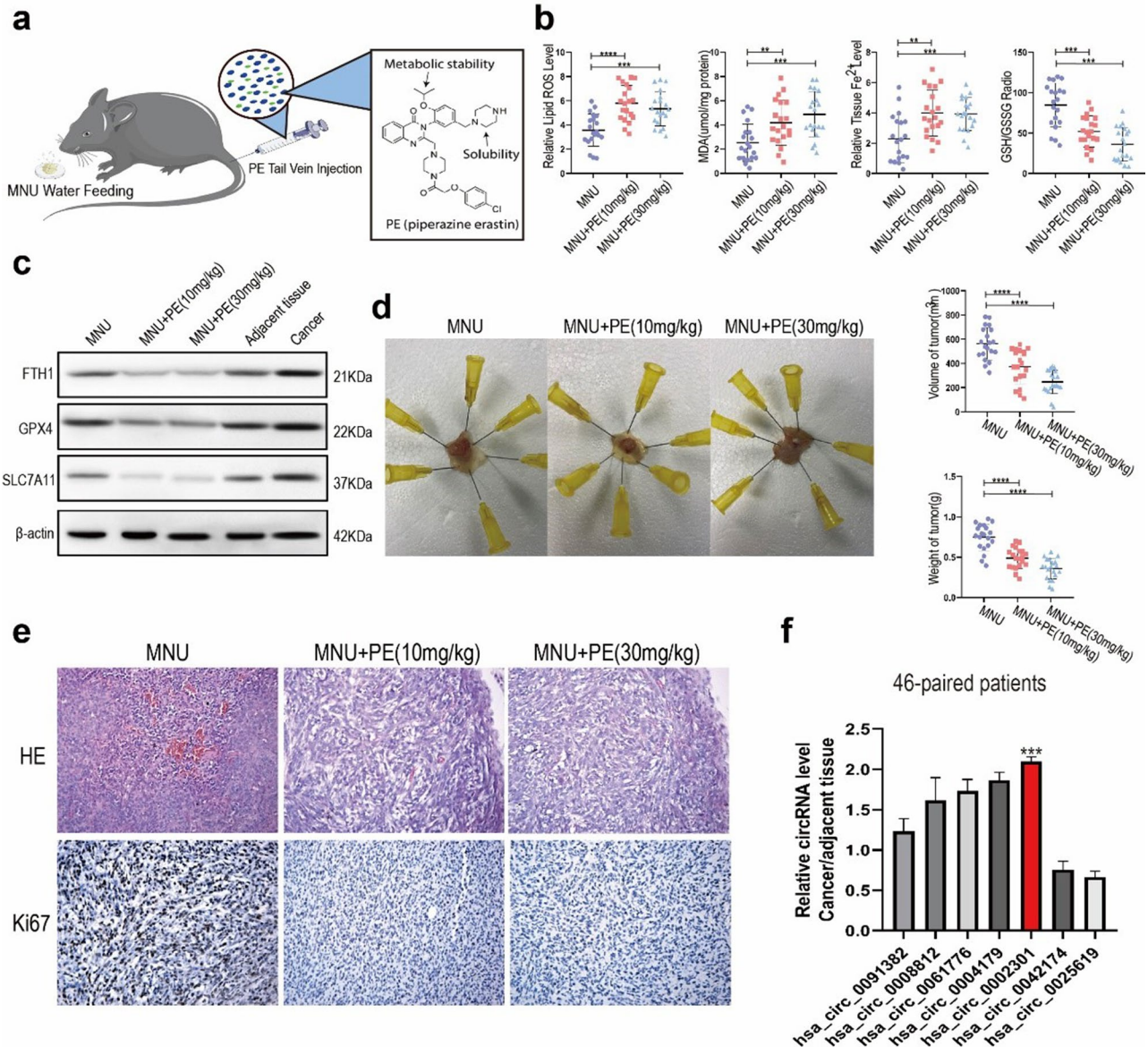


**Fig. 1** Elevated hsa_circ_0002301 expression is correlated with ferroptosis in a gastric cancer model.**a.** A mouse gastric cancer model induced by N-methyl-N-nitrosourea (MNU) was established. **b.** Ferroptosis indicators, such as $Fe^{2+}$ accumulation, MDA levels, ROS levels, and the GSH/GSSG ratio, were assessed in the three groups. **c**. FNR protein expression was assessed in adjacent nontumor tissues and gastric cancer tissues from mice. **(d)** Tumor sections were spread for volume and weight measurements. **(e)** Hematoxylin and eosin (H&E) staining revealed the histopathological morphology of gastric cancer tissues with high ferroptosis levels, while Ki-67 staining revealed the cell proliferation capacity. Scale bar: 100 μm. **(f)** Expression of the 7 selected circRNAs in 46 pairs of gastric cancer and adjacent tissues from clinical samples obtained during surgery. The graph shows the mean ± standard deviation (SD) values; *$p < 0.05$, **$p < 0.01$, and ***$p < 0.001$

significant decrease in the proliferative capacity (Fig. 1e). Collectively, these findings suggest that ferroptosis can effectively inhibit the initiation and progression of gastric cancer.

We and others have previously shown that circRNAs play important roles in gastric cancer [30–32]. Hence, we predicted the coding potential of 236 circRNAs differentially expressed between human gastric cancer and adjacent tissues using the sequencing dataset GSE163416 (Table S1). Among these circRNAs, 7 could encode peptides (hsa_circ_0091382, hsa_circ_0008812, hsa_circ_0061776, hsa_circ_0004179, hsa_circ_0002301, hsa_circ_0042174, and hsa_circ_0025619) (Fig. S1a) wand were considered for further investigation. qRT–PCR was performed to analyze the differences in the expression of these circRNAs in 46 pairs of gastric cancer and adjacent tissues. Among the seven screened circRNAs, hsa_circ_0002301, hsa_circ_0004179, and hsa_circ_0061776 were notable as the circRNAs with the most significant differences in expression in these

clinically surgically resected samples (Fig. 1f). We further analyzed the expression of these circRNAs in gastric cancer tissue samples from mice treated with PE. The levels of hsa_circ_0002301 were significantly different in both peripheral blood and gastric cancer tissues from tumor-bearing mice with and without PE induction (Fig. S1b). Furthermore, this study confirmed the correlation between the levels of ferroptosis and hsa_circ_0002301 expression in 60 gastric cancer tissues and the size and volume of the corresponding tumors (Fig. S1c; Table S2). These findings suggest that hsa_circ_0002301 is involved in the progression of gastric cancer and is closely associated with ferroptosis.

#### Hsa_circ_0002301 modulates biological functions in gastric cancer cells in a ferroptosis-dependent manner

Hsa_circ_0002301 was found to have a total length of 1403 nucleotides and originated from exons 23, 24, 25, and 26 of HECTD1 located on chromosome 14 (Fig. 2a). Sanger sequencing verified the head-to-tail junction of the amplified hsa_circ_0002301 sequence (Fig. 2b). Divergent and convergent primers were designed to confirm that hsa_circ_0002301 formed by reverse splicing of exons. Divergent and convergent primers were designed for this study, with complementary DNA (cDNA) and genomic DNA (gDNA) extracted from MKN45 cells used as templates. The gel electrophoresis results indicated that hsa_circ_0002301 was amplified only from cDNA and not from gDNA (Fig. S2a). Furthermore, after treatment with actinomycin D (a transcription inhibitor), hsa_circ_0002301 exhibited a significantly longer half-life than the HECTD1 mRNA, demonstrating the stability of hsa_circ_0002301 (Fig. S2b). Subsequent fluorescence in situ hybridization (FISH) (Fig. 2c) and qRT−PCR analyses (Fig. 2d) of gastric cancer cells revealed that hsa_circ_0002301 was distributed in both the cytoplasm and nucleus, with predominant localization in the cytoplasm. PCR was performed to assess the expression of hsa_circ_0002301 in gastric cancer tissues relative to that in matched adjacent gastric cancer tissues from 90 patients. We generated overall survival (OS) curves using the Kaplan−Meier survival analysis based on survival data from patients with previous follow up. The results revealed that patients with higher levels of hsa_circ_0002301 in gastric cancer tissues experienced significantly shorter overall survival (Fig. 2e). In conclusion, our results suggest that hsa_circ_0002301 is stably expressed in gastric cancer cells and has potential prognostic utility in gastric cancer.

We assessed the expression of hsa_circ_0002301 in both normal gastric tissues and multiple gastric cancer cell lines to investigate the impact of hsa_circ_0002301 on the biological function of gastric cancer cells. The highest expression of hsa_circ_0002301 was detected in MKN45 and HGC27 cells and the lowest expression in AGS and MKN28 cells (Fig. S2c). Unlike the linear mRNA of the host gene HECTD1, hsa_circ_0002301 displayed resistance to ribonuclease R (RNase R) degradation, confirming the high stability of this circRNA (Fig. S2d). These siRNAs were then introduced into the MKN45 and HGC27 cell lines, which presented higher hsa_circ_0002301 levels than the other tested gastric cancer cell lines. Additionally, the AGS and MKN28 cell lines, characterized by lower hsa_circ_0002301 expression levels, were transfected with plasmids for hsa_circ_0002301 overexpression. The silencing efficiency of the designed hsa_circ_0002301 siRNAs and the transfection efficiency of the hsa_circ_0002301 overexpression plasmid were validated by qRT–PCR, which showed the effective silencing and overexpression of hsa_circ_0002301, with no effect on the mRNA expression of the parental gene HECTD1 (Fig. S2e-f). We observed that hsa_circ_0002301 increased proliferation (Fig. 2f), invasion (Fig. 2g-h), and migration (Fig. 2i) and decreased apoptosis (Fig. S2g-h) in gastric cancer cells. The modulation of hsa_circ_0002301 expression also regulated cell cycle progression in gastric cancer cells (Fig. S2i-j).

Furthermore, we examined the changes in ferroptosis in gastric cancer cells with hsa_circ_0002301 knockdown or overexpression compared with the corresponding control cells. After hsa_circ_0002301 knockdown, pathological mitochondrial characteristics, including mitochondrial shrinkage and an increased mitochondrial membrane density, were observed (Fig. 3a). Moreover, when lipid ROS and MDA levels increased, iron ($Fe^{2+}$) accumulation occurred and the GSH/GSSG ratio decreased, collectively indicating that hsa_circ_0002301 knockdown induced cellular ferroptosis (Fig. 3b). Conversely, overexpression of hsa_circ_0002301 resulted in the opposite effects (Fig. 3a-b). In agreement, morphological observations under inverted phase-contrast microscopy identified a distinct “ballooning” phenotype in treated MKN45 and HGC27 cells (Fig. S3a). Cells in which hsa_circ_0002301 was silenced or overexpressed were treated with either the ferroptosis inhibitor Fer-1 or the ferroptosis inducer erastin. The results revealed that when ferroptosis was induced, the previously observed oncogenic effects of hsa_circ_0002301 overexpression on gastric cancer cells were abolished. Conversely, when ferroptosis was inhibited, hsa_circ_0002301 knockdown failed to restore the malignant biological behavior of gastric cancer cells (Fig. 3c-i). Furthermore, to investigate whether other forms of cell death, apart from ferroptosis, contribute to the observed mortality of gastric cancer cells in this context, we treated the cells with specific inhibitors targeting apoptosis (Z-VAD-FMK), necroptosis (necrostatin-1), and autophagy (chloroquine). The results demonstrated that inhibition of apoptosis,

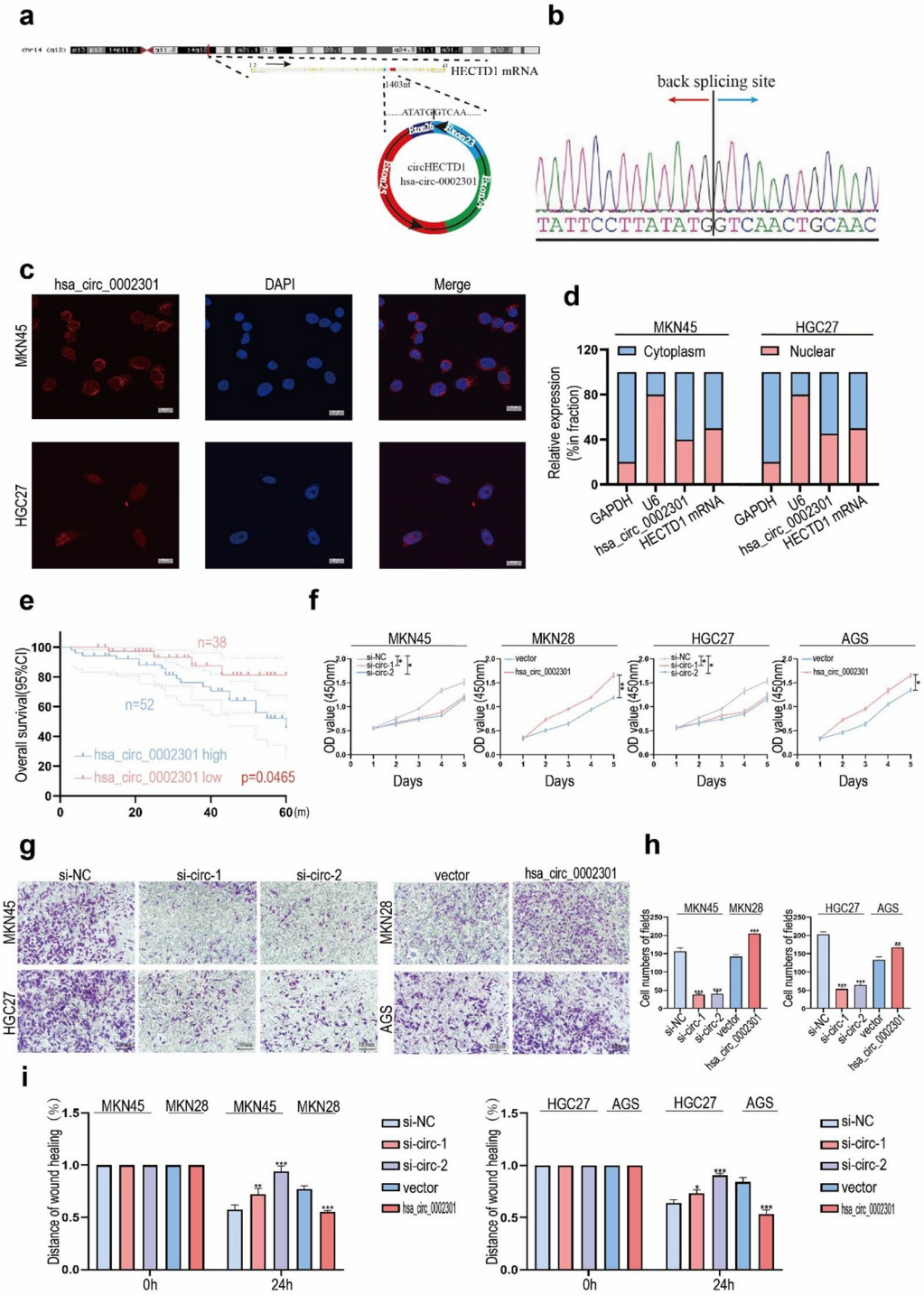


**Fig. 2** Hsa_circ_0002301 modulates biological functions in gastric cancer cells in a ferroptosis-dependent manner.**(a)** Schematic representation showing that hsa_circ_0002301 is derived from exons 23, 24, 25, and 26 of HECTD1 **(b)** Head-to-tail splicing was confirmed by Sanger sequencing. **(c)** FISH results demonstrated that hsa_circ_0002301 was distributed within both the cytoplasm and nucleus. Scale bar: 20 μm. **(d)** Nuclear–cytoplasmic fractionation revealed that hsa_circ_0002301 was distributed in both the cytoplasm and the nucleus, with predominant localization in the cytoplasm. **(e)** Overall survival analysis of 90 patients with GC stratified by hsa_circ_0002301 expression. **(f)** A Cell Counting Kit-8 (CCK-8) assay was performed to assess the proliferative capacity of GC cells following the upregulation or downregulation of hsa_circ_0002301. **g**, **h.** Transwell assays were performed to investigate the influence of hsa_circ_0002301 on cell invasion. **i.** Wound healing assays were performed to assess the migratory ability of GC cells following the upregulation or downregulation of hsa_circ_0002301. The graph shows the mean ± SD values; * $P < 0.05$, ** $P < 0.01$, and *** $P < 0.001$

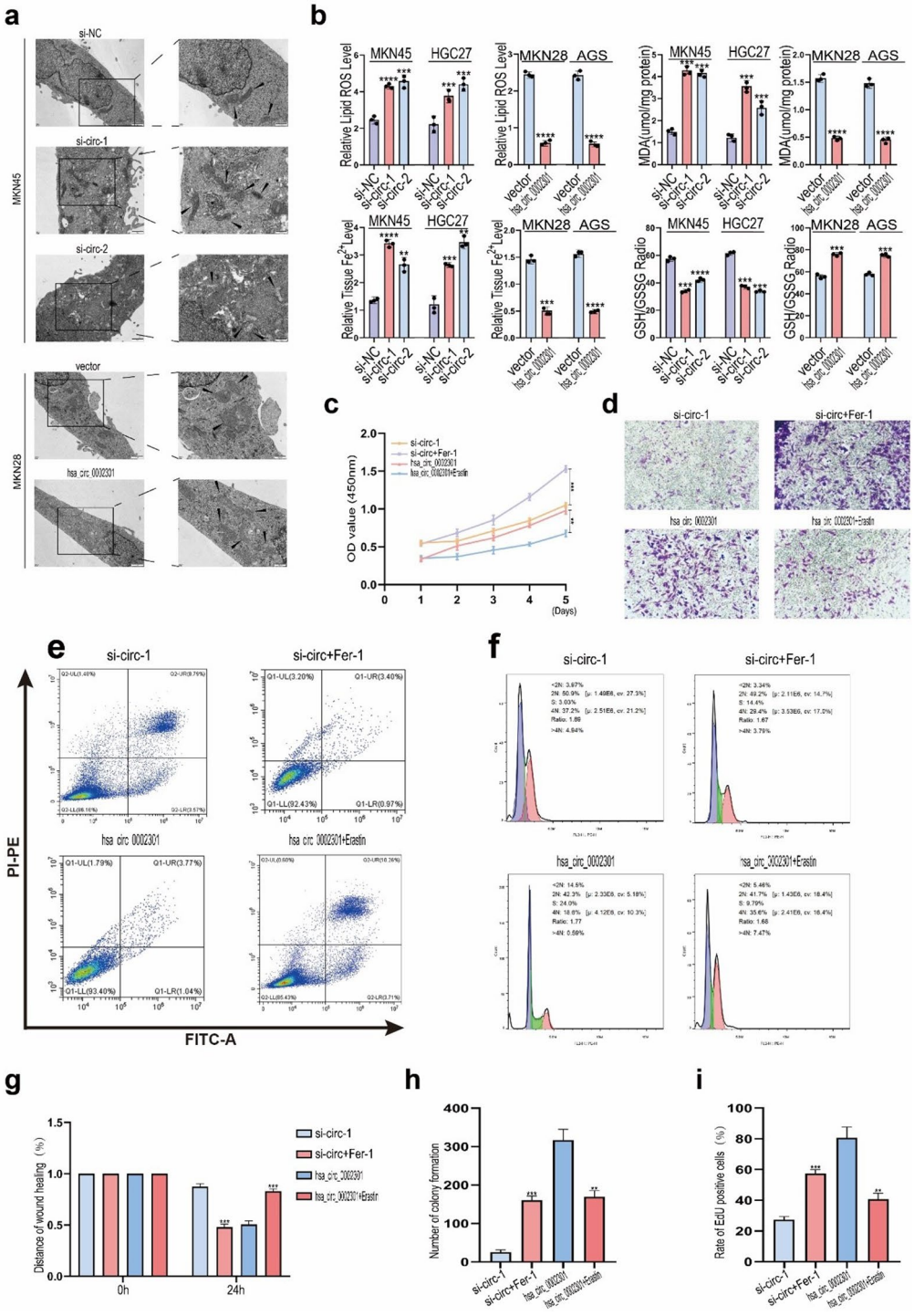


**Fig. 3** Hsa_circ_0002301 regulates the biological functions of gastric cancer cells through the modulation of ferroptosis. **(a)** Transmission electron microscopy was used to examine the impact of the upregulation or downregulation of hsa_circ_0002301 on organelle morphology (ferroptosis level) in GC cells. Scale bars: 1 μm and 500 nm. **(b)** The levels of lipid ROS, MDA, and $Fe^{2+}$ and the GSH/GSSG ratio in GC cells were determined after the upregulation or downregulation of hsa_circ_0002301. **c-i.** When hsa_circ_0002301 was upregulated or downregulated and cells were treated with either Fer-1 or erastin, the effects on GC cell proliferation, invasion, apoptosis, and cell cycle progression were assessed. The graph shows the mean ± SD values; *$p < 0.05$, **$p < 0.01$, and ***$p < 0.001$

necroptosis, or autophagy did not significantly alter the regulatory effect of hsa_circ_0002301 on ferroptosis in gastric cancer cells (Fig. S4a, b). Therefore, our findings support the hypothesis that hsa_circ_0002301 affects the ferroptosis-dependent initiation and progression of gastric cancer.

### Hsa_circ_0002301 encodes a specific 463 amino acid peptide, HECTD1-463aa

Emerging evidence has highlighted the peptide-encoding capacity of several circRNAs [33, 34]. Based on the information provided by circRNADb, catRAPID, RBPDB, and CircAtla, possible open reading frames (ORFs) and internal ribosome entry sites (IRESs) were predicted (Fig. S5a). These predicted data suggested that hsa_circ_0002301 encodes a specific peptide of 463 amino acids, which we termed HECTD1-463aa in this study (Fig. 4a). The dual-luciferase assay revealed significantly higher luciferase activity driven by the wild-type IRES encompassing nucleotides 4–151 (IRES-1) than by the wild-type IRES encompassing nucleotides 573–720 and either mutant IRES. In other words, the IRES encompassing nucleotides 4–151 exhibited the strongest activity (Fig. 4b). We designed and synthesized a polyclonal antibody targeting the middle portion of HECTD1-463aa (240 aa–387 aa) to detect this novel protein (Fig. 4a, right panel). Western blots showed increased HECTD1-463aa expression in gastric cancer tissues compared with normal gastric tissues, whereas HECTD1 expression was not substantially changed (Fig. 4c; Fig. S6b).

We introduced hsa_circ_0002301 expression plasmids with mutations in IRES-1 and hsa_circ_0002301 overexpression plasmids into HEK-293T cells. Silver staining revealed a distinct protein band at approximately 55 kDa, precisely matching the predicted size of HECTD1-463aa (Fig. 4d, right panel). We constructed an overexpression plasmid with a Flag sequence immediately upstream of the stop codon of hsa_circ_0002301 (hsa_circ_0002301-Flag). Validation through qRT-PCR and Western blot analyses confirmed the successful expression of HECTD1-463aa-Flag, which was introduced into 293T cells. Subsequent Western blot results revealed that an anti-Flag antibody could detect the newly translated protein, confirming that hsa_circ_0002301 has protein-coding ability. We subsequently purified the newly translated protein by immunoprecipitation (IP) using an anti-FLAG antibody for further validation. LC–MS/MS results indicated the presence of a specific sequence for the predicted 55-kDa peptide (Fig. 4d, left panel), confirming that HECTD1-463aa was indeed translated from hsa_circ_0002301. Furthermore, immunofluorescence (IF) staining with an anti-Flag antibody confirmed that HECTD1-463aa was localized primarily in the cytoplasm of MKN45 cells (Fig. 4e). An in-depth Kaplan–Meier survival analysis indicated that gastric cancer patients with higher HECTD1-463aa expression experienced significantly shorter overall survival times than those with lower HECTD1-463aa expression (Fig. 4f).

We subsequently measured ferroptosis levels in MKN28 and AGS cells overexpressing HECTD1-463aa and with HECTD1 knockdown. Compared with the corresponding control conditions, both HECTD1-463aa overexpression and HECTD1 knockdown led to decreased lipid ROS levels and MDA depletion, reduced $Fe^{2+}$ accumulation, and an increased GSH/GSSG ratio in gastric cancer cells (Fig. S5b).

### HECTD1-463aa interacts with HECTD1 to inhibit ferroptosis in gastric cancer

To further ascertain the biological function of HECTD1-463aa, We observed organelle morphology in MKN45 cells using electron microscopy to further investigate the biological function of HECTD1-463aa, and the results revealed that the overexpression of HECTD1-463aa in gastric cancer cells led to a reduction in ferroptosis (Fig. 5a-b). These findings indicate that HECTD1-463aa suppresses ferroptosis in gastric cancer cells.

Co-IP was performed with an anti-Flag antibody to pull down proteins that interact with HECTD1-463aa-Flag and to elucidate the specific mechanism by which HECTD1-463aa regulates ferroptosis in gastric cancer. We then performed a qualitative analysis using LC–MS/MS on the proteins obtained by co-IP. HECTD1 was one of the proteins that immunoprecipitated with HECTD1-463aa-Flag (Fig. 5c). This interaction was subsequently verified through co-IP and Western blot analyses, confirming the binding between HECTD1-463aa and HECTD1 (Fig. 5d; Fig. S6c). Moreover, we performed immunofluorescence staining with an anti-Flag antibody for the colocalization analysis. Immunofluorescence staining revealed that HECTD1-463aa colocalized with HECTD1 in the cytoplasm (Fig. 5e). We generated a Flag mutant that lacked the unique new peptide segment (HECTD1-463aa-Δspecific a.a-Flag) and another Flag mutant containing only the new peptide segment (specific a.a-Flag) to investigate the possible region of HECTD1-463aa that interacted with HECTD1. The co-IP results showed that only the HECTD1-463aa mutant containing the specific a.a. segment and the full-length HECTD1-463aa protein could interact with the HECTD1 protein (Fig. 5f).

### HECTD1 regulates GPX4 ubiquitination, with far-reaching effects on ferroptosis in gastric cancer

Our previous research demonstrated that hsa_circ_0002301 can modulate the biological functions of gastric cancer cells by regulating ferroptosis and modulating the level of the FNR gene GPX4 [35, 36]. Building

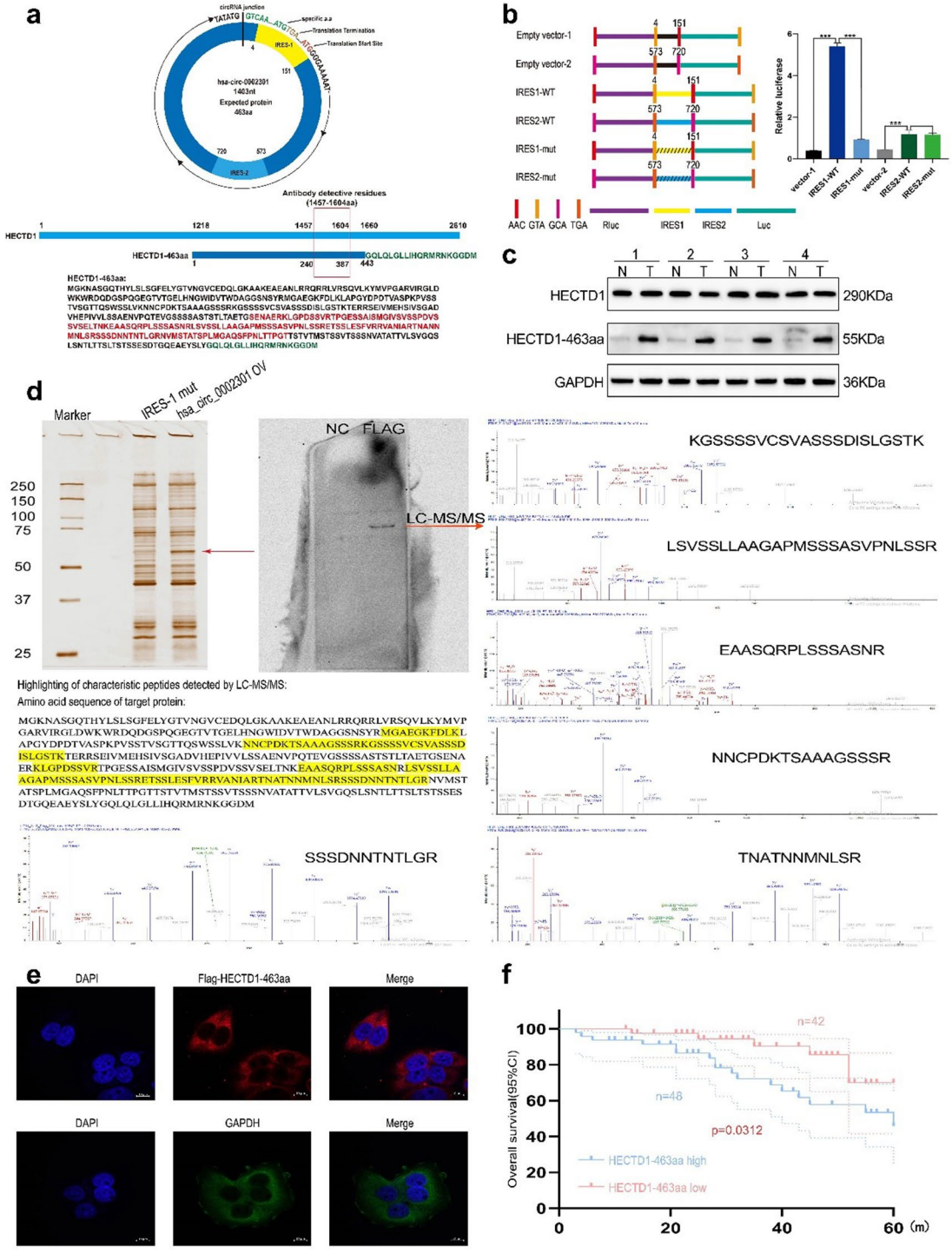


**Fig. 4** Characterization of the protein HECTD1-463aa encoded by hsa_circ_0002301. **(a)** Structural schematic representation of the predicted IRES region and ORF in hsa_circ_0002301. **(b)** Left panel: the wild-type or mutant IRES was inserted between the Rluc and Luc reporter genes, each with an independent start and stop codon. Right panel: the relative luciferase activity was measured. The graph shows the mean ± SD values; *$p < 0.05$, **$p < 0.01$, and ***$p < 0.001$. **(c)** The expression of HECTD1-463aa in 4 pairs of gastric cancer and adjacent tissues was examined using Western blotting. **(d)** Total protein from HEK-293T cells transfected with the hsa_circ_0002301 and IRES-1 mut plasmids was separated by SDS–PAGE. The overexpression of HECTD1-463aa was confirmed by immunoblotting. Gel bands containing proteins with molecular weights between 50 kDa and 75 kDa were excised and subjected to LC–MS/MS analysis. The amino acids identified in HECTD1-463aa are highlighted in yellow. **(e)** HECTD1-463aa-Flag was transfected into MKN45 cells. Immunofluorescence staining was performed using an anti-Flag antibody to visualize the cellular localization of HECTD1-463aa. Scale bar: 10 μm. **(f)** Overall survival analysis based on the expression of HECTD1-463aa in 90 gastric cancer patients

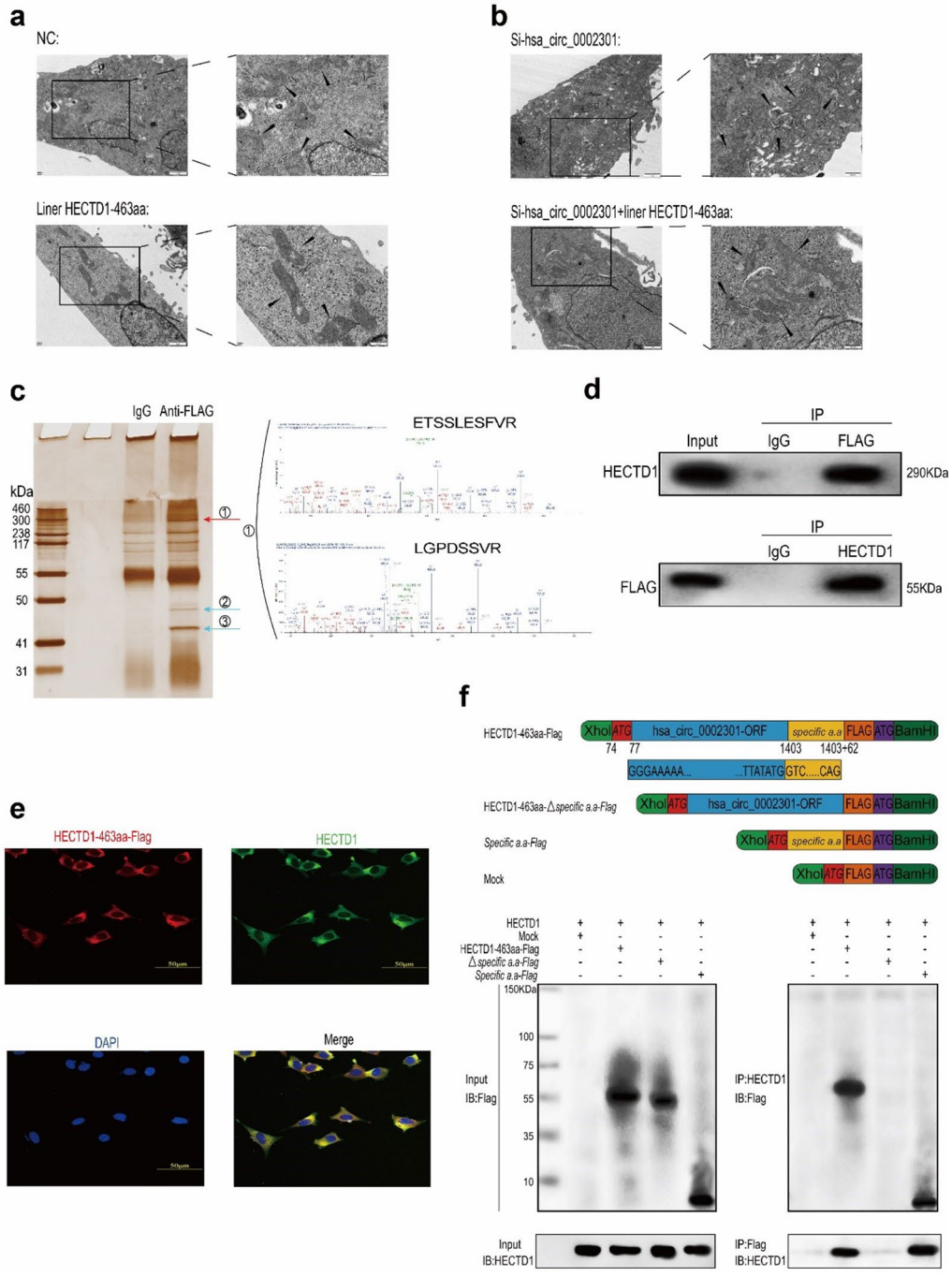


**Fig. 5** HECTD1-463aa interacts with HECTD1 to inhibit ferroptosis in gastric cancer. **a**, **b.** Transmission electron microscopy was employed to assess the impact of HECTD1-463aa upregulation or hsa_circ_0002301 downregulation on organelle morphology (ferroptosis) in GC cells. Scale bars: 1 μm and 500 nm. **c.** Total protein from HEK293T cells transfected with the HECTD1-463aa-Flag plasmid was separated by SDS–PAGE. LC–MS/MS analysis was then performed. The arrow indicates distinct bands between the IgG and Flag lanes. **d.** The mutual interaction between HECTD1 and HECTD1-463aa is shown by IP. **e.** Immunofluorescence staining shows the colocalization of HECTD1-463aa and HECTD1 in the cytoplasm. **f.** The upper panel shows a schematic representation of the constructed FLAG mutant. The lower panel shows the results of the co-IP experiments exploring the interactions of the mutant. The graph shows the mean ± SD values; * $P < 0.05$, ** $P < 0.01$, and *** $P < 0.001$

on this observation, we analyzed publicly available data from TCGA to investigate the relationship between GPX4 expression and the long-term survival of gastric cancer patients. The results indicated that patients with low GPX4 expression had significantly higher long-term survival rates (Fig. 6a). The GEPIA database was subsequently used to assess the correlation between the expression of GPX4 and HECTD1, and a negative correlation was found, suggesting that HECTD1 could exert an inhibitory effect on GPX4 (Fig. 6b). Thus, we designed a short hairpin RNA (shRNA) specifically targeting hsa_circ_0002301 (sh-hsa_circ_0002301) to stably knock down HECTD1-463aa, thus allowing the investigation of the relationship between HECTD1-463aa and HECTD1. IP experiments revealed that in MKN45 and HGC27 cells with stable HECTD1-463aa knockdown, the binding between GPX4 and HECTD1 increased compared to that in the corresponding control cells. In MKN28 and AGS cells, HECTD1-463aa overexpression significantly reduced the interaction between GPX4 and HECTD1 (Fig. 6c; Fig. S7a). These results suggest that HECTD1-463aa suppresses HECTD1 binding to GPX4.

MKN45 and HGC27 cells were treated with cycloheximide (CHX) in combination with sh-hsa_circ_0002301 to assess the effect of hsa_circ_0002301 knockdown on GPX4 protein stability. The experimental results revealed a noticeable reduction in GPX4 protein stability over time following hsa_circ_0002301 knockdown, suggesting that hsa_circ_0002301 may play a role in the degradation of GPX4 in gastric cancer cells. However, further experiments showed that the overexpression of HECTD1-463aa following hsa_circ_0002301 knockdown restored GPX4 protein stability. However, the overexpression of hsa_circ_0002301 with a mutated IRES-1 sequence was unable to restore the stability of the GPX4 protein (Fig. 6d; Fig. S7b). These findings indicate that the regulatory factor involved in controlling GPX4 protein degradation is HECTD1-463aa.

### In vivo validation of the role of hsa_circ_0002301 in gastric cancer progression and its clinical significance

We investigated the role of hsa_circ_0002301 in tumorigenicity in vivo to corroborate our in vitro findings. Previously, stable hsa_circ_0002301-silenced MKN45 and HGC27 cell lines were generated. These stable cells were subcutaneously implanted into nude mice, and the growth of the subcutaneous tumors was monitored weekly. Silencing hsa_circ_0002301 significantly inhibited tumor growth. Compared with the control, HECTD1-463aa overexpression significantly promoted tumor growth in gastric cancer cells (Fig. 7a). H&E and Ki67 staining revealed fewer pathological lesions and weaker proliferation marker signals in the hsa_circ_0002301 knockdown group than in the control group. Consistent with the trend in tumor size, overexpression of HECTD1-463aa resulted in opposite changes and partially reversed the effects of hsa_circ_0002301 silencing (Fig. 7b). We measured the expression levels of hsa_circ_0002301 relative to those in matched adjacent gastric cancer tissues from 90 patients using qRT–PCR. We collected and analyzed clinical data related to hsa_circ_0002301 expression, revealing significant positive correlations between high hsa_circ_0002301 expression and a large tumor size, lymphatic invasion, high TNM stage, and hematogenous metastasis (Fig. 7c). In conclusion, we discovered that HECTD1-463aa suppresses the HECTD1-mediated ubiquitination of GPX4 (Fig. 7d).

## Discussion

Ferroptosis, a form of cell death triggered by metabolic stress, is characterized by the depletion of cysteine and iron-dependent accumulation of excessive lipid ROS [37, 38]. The process of circRNA regulation in gastric cancer progression is extraordinarily intricate. We chose the mechanism by which circRNAs encode proteins as our starting point to investigate the role of circRNAs in the development of gastric cancer from the perspective of ferroptosis. CircRNAs are a special class of noncoding RNAs with a circular structure that are not subjected to the 5' to 3' end degradation pathway of linear RNAs and are therefore relatively stable [39]. Although circRNAs were once thought to be noncoding RNAs, recent studies have shown that certain circRNAs have the ability to encode small peptides [40]. These small peptides may have important biological functions within cells. Compared with other studies conducted horizontally, most studies on circRNAs in tumors have focused on their roles as miRNA sponges or in the regulation of parental gene expression [30]. Currently, no cases of circRNAs regulating the level of ferroptosis in gastric cancer by encoding proteins have been reported. Based on the naturally occurring gastric cancer model in mice induced by MNU, we employed the ferroptosis inducer erastin analog piperazine erastin (PE), which is suitable for in vivo experiments, to induce ferroptosis during the development of gastric cancer [41–43]. This study is the first to explore the role of ferroptosis in the process of gastric cancer development [44]. Moreover, cellular death mechanisms are highly diverse and often exhibit overlapping or interdependent regulatory pathways. To elucidate the specificity of hsa_circ_0002301 in modulating ferroptosis, we employed inhibitors targeting alternative cell death modalities, including apoptosis (Z-VAD-FMK), necroptosis (necrostatin-1), and autophagy (chloroquine) [11, 28].Our findings revealed that hsa_circ_0002301 specifically regulates ferroptosis without significant crosstalk from these alternative cell death pathways, underscoring its unique role in ferroptosis regulation. These results

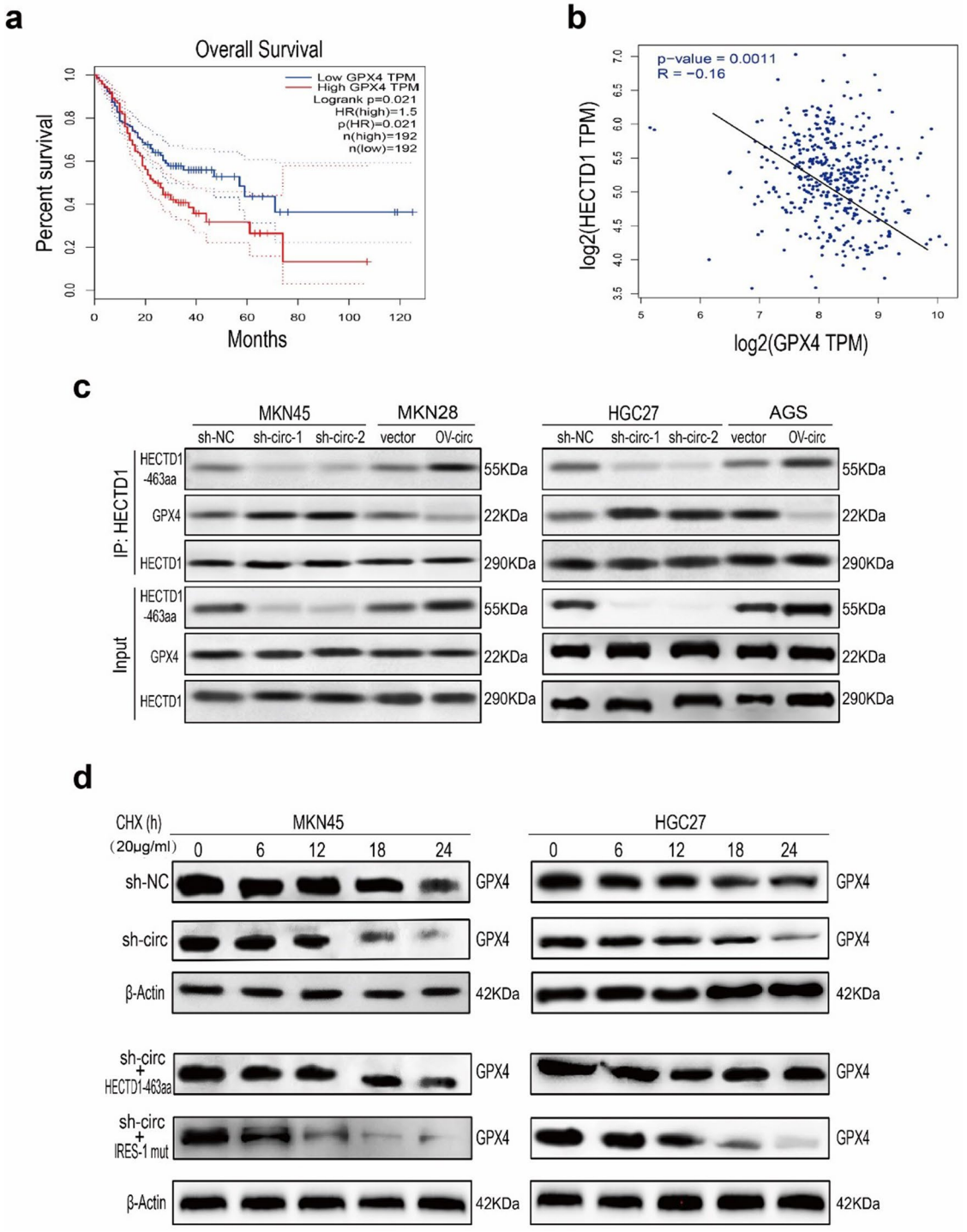


**Fig. 6** HECTD1 regulates GPX4 ubiquitination, with far-reaching effects on ferroptosis in gastric cancer. **(a)** The relationship between GPX4 and the long-term survival rate of gastric cancer patients was analyzed using the public The Cancer Genome Atlas (TCGA) database. **(b)** The correlation between GPX4 and HECTD1 gene expression was analyzed using the GEPIA database. **(c)** In MKN45 and HGC27 cell lines with stable hsa_circ_0002301 knockdown, the relationship between HECTD1 and GPX4 was observed by performing IP experiments combined with WB experiments. **(d)** Protein biosynthesis in GC cells was blocked with 20 μg/mL cycloheximide (CHX). Western blot analysis was conducted at various time points to assess the GPX4 protein levels in GC cells with hsa_circ_0002301 downregulation or HECTD1-463aa upregulation

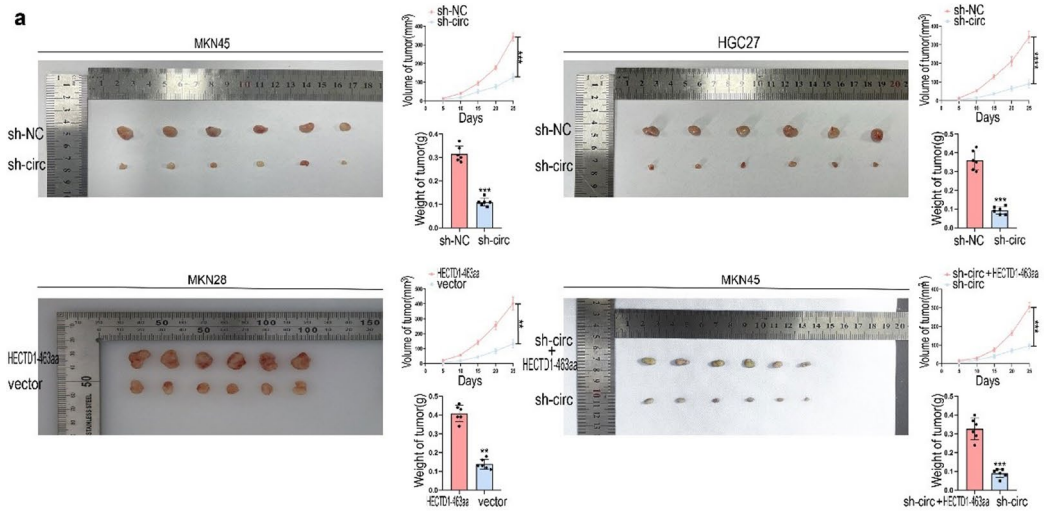


c

Baseline characteristics of GC patients

| Characteristics | N=90(%) | hsa_circ_0002301 low(n=38) | hsa_circ_0002301 high(n=52) | p Value |
|---|---|---|---|---|
| Gender | | | | 0.078 |
| Male | 62(68.9%) | 30(78.9%) | 32(61.5%) | |
| Female | 28(31.1%) | 8(21.1%) | 20(38.5%) | |
| Age，years | | | | 0.051 |
| ≤50 | 46(51.1%) | 24(63.2%) | 22(42.3%) | |
| >50 | 44(48.9%) | 14(36.8%) | 30(57.7%) | |
| Tumor size | | | | 0.0041* |
| ≤3 | 30(33.3%) | 19(50%) | 11(21.1%) | |
| >3 | 60(66.7%) | 19(50%) | 41(78.9%) | |
| Lymph node metastasis | | | | 0.0115* |
| N0 | 36(40%) | 21(55.3%) | 15(28.8%) | |
| N1-N3 | 54(60%) | 17(44.7%) | 37(71.2%) | |
| TNM stage | | | | 0.0125* |
| I-II | 43(47.8%) | 24(63.2%) | 19(36.5%) | |
| III | 47(52.2%) | 14(36.8%) | 33(63.5%) | |
| Blood vessel invasion | | | | 0.0140* |
| Negative | 58(64.4%) | 30(78.9%) | 28(53.9%) | |
| Positive | 32(35.6%) | 8(21.1%) | 24(46.1%) | |

*p<0.05

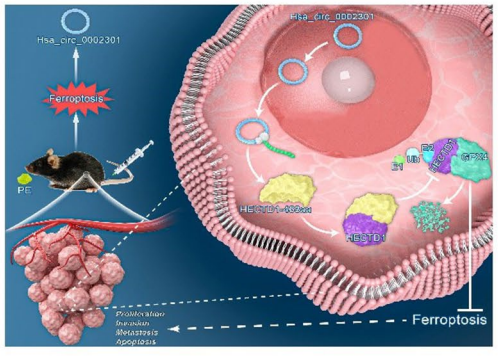


**Fig. 7** In vivo validation of the role of hsa_circ_0002301 in gastric cancer progression and its clinical significance. **(a)** The specified tumor cells were subcutaneously injected into nude mice. Tumor volumes were measured weekly, and tumor weights were recorded at 28 days postinjection. **(b)** H&E staining and Ki67 immunostaining were performed according to the previous grouping scheme. Scale bars: 500 μm and 50 μm. **(c)** Correlations between hsa_circ_0002301 expression and clinicopathological parameters in 90 GC patients. *$p < 0.05$, **$p < 0.01$, and ***$p < 0.001$. **(d)** Mechanistic model showing the proposed role of hsa_circ_0002301 in GC. HECTD1-463aa inhibits the ubiquitination of GPX4 by binding to HECTD1

were consistently replicated across multiple experiments, ensuring robustness and reproducibility in alignment with established methodologies for studying cell death mechanisms. This specificity highlights the distinct functional contribution of hsa_circ_0002301 to ferroptosis, independent of other cell death processes.

The newly encoded protein HECTD1-463aa competitively binds to the E3 ubiquitin ligase HECTD1, inhibiting the degradation of GPX4. Recently, several ncRNAs, particularly circRNAs, miRNAs, and lncRNAs, have been reported to participate in the biological processes of ferroptosis, thereby impacting tumor growth. However, the precise regulatory mechanisms underlying this phenomenon remain to be elucidated [45]. A disruption of ferroptosis can contribute to cancer progression. Emerging research has indicated that circRNAs featuring IRESs or extensive methylation may influence physiological behaviors via protein-coding functions, thereby providing a novel perspective on their potential contributions to gastric cancer progression [18, 19]. Owing to their distinctive circular structure, circRNAs may undergo multiple rounds of translation when bound to ribosomes, potentially generating unique peptide segments whose amino acid sequences differ from those of the host gene-encoded proteins [20]. The emergence of novel amino acid sequences increases the likelihood that a newly synthesized protein possesses functions distinct from those of the host gene-encoded protein [46–48]. Based on the results reported in the literature, most of the regulatory effects of circRNAs on ferroptosis in cancer cells are achieved primarily through sequestration of miRNAs, which consequently influences the expression of ferroptosis-related proteins [49, 50]. However, the pattern of protein–protein interactions is more complex and intriguing than the pattern of circRNA–miRNA interactions. To our knowledge, this study is the first to reveal a novel mechanism. Whether this mechanism, where a circRNA formed by the retrotranscription of a parent gene antagonizes the function of the protein encoded by the same gene, holds general applicability remains to be explored. Additionally, whether other mechanisms regulate the formation of circRNAs and subsequently influence the function of the parent gene is worthy of further investigation [51]. The discovery of oncogenic circRNAs with protein-coding capabilities that antagonize the parent gene may represent a novel direction for tumor therapy.

HECTD1 is a member of the Hect family, which plays a crucial role in regulating substrate protein degradation through the ubiquitination pathway. Previous studies have indicated the significant involvement of HECTD1 in biological processes such as embryonic development, cell cycle regulation, and tumor suppression [52]. Earlier research has suggested its critical role in neural tube and organ development during embryonic development, as well as its involvement in regulating the G1/S and G2/M transitions in the cell cycle. Furthermore, some studies, which have focused primarily on breast cancer, have implicated HECTD1 in the occurrence and development of certain tumors [53, 54]. In addition, recent findings suggest that the ubiquitination activity of HECTD1 may be linked to specific signaling pathways, such as the Wnt/β-catenin and Notch pathways [55]. This observation provides new insights into the role of HECTD1 in cellular signal regulation [56, 57]. Additionally, emerging analyses and experimental techniques, such as proteomic analysis and gene editing, offer powerful tools for further revealing the functions and regulatory mechanisms of HECTD1.

Our study is an important addition to the function of hsa_circ_0002301, a key molecule that regulates the malignant behavior of gastric cancer, and can be used to construct a network of mechanisms by which individual circRNAs regulate the progression of gastric cancer, which can provide a comprehensive and complete basic theory of this circRNA as a clinical diagnostic and therapeutic target in the future.

## Conclusions

In this study, we elucidated a novel mechanism by which hsa_circ_0002301 influences gastric cancer. This circular RNA encodes the HECTD1-463aa protein, which competitively inhibits the function of its parental gene HECTD1. Consequently, it attenuates the degradation of GPX4, thereby exerting an effect on the ferroptosis of gastric cancer cells. Notably, the suppressive effect of hsa_circ_0002301 on iron deficiency in gastric cancer cells plays a pivotal role in the onset, progression, and various malignant behaviors of gastric cancer cells. This mechanism is the key to controlling ferroptosis in gastric cancer cells.

In particular, the discovery of the role of hsa_circ_0002301 as a key mediator regulating GPX4 ubiquitination and expression provides new opportunities for the development of therapeutic approaches for gastric cancer. Given the identification of this dual regulatory mechanism, this research could pave the way for further breakthroughs in cancer treatment and development.

## Methods

### Cell culture and treatment

Cell lines, including BGC-823, MKN28, MGC803, MKN-45, HGC-27, and AGS cells, were obtained from the Center Laboratory at Yijishan Hospital, Wannan Medical College, and were authenticated. The human gastric cell lines were cultured in RPMI 1640 (Gibco, USA) at 37 °C with 5% carbon dioxide in an incubator. HEK-293T cells were procured from the China Center for Type Culture

Collection (CCTCC, Shanghai, China) and cultured in Dulbecco's modified Eagle's medium (DMEM). All the cell lines were maintained in a humidified incubator at 37 °C with 5% $CO_2$ and 95% air. DMEM (Thermo Fisher Scientific, Waltham, MA, USA) containing 10% fetal bovine serum (FBS) (Gibco, NY, USA) and 1% penicillin–streptomycin was used. Notably, all the cell lines tested negative for mycoplasma contamination.

#### Patients and tissue samples

Between 2015 and 2017, 90 pairs of human gastric cancer and adjacent nontumor tissues were collected at the Digestive Center of the First Affiliated Hospital of Wannan Medical College. This study was approved by the Clinical Research Ethics Committee of the First Affiliated Hospital of Wannan Medical College (WNMC-AWE-2023287). All the participants provided written informed consent. This study was conducted in accordance with the Declaration of Helsinki (https://www.wma.net/what-we-do/medical-ethics/declaration-of-helsinki/).

The clinicopathological characteristics analyzed included age, sex, tumor size, tumor location, lymph node metastasis status, TNM stage (according to the American Joint Committee on Cancer (AJCC) guidelines), and vascular invasion status, as shown in Fig. 7c.

#### qRT–PCR

Total RNA was extracted from the tissues and cells using the TRIzol method. A total of 2 μg of RNA was reverse transcribed into cDNA after the addition of 5× PrimeScript RT Master Mix and thorough mixing. For qRT–PCR, 1μL of cDNA was mixed with 2×SYBR Green Mix (5μL) and the corresponding primers, and the final reaction volume was adjusted to 20μL. Each well was supplemented with 0.8μL each of the upstream and downstream primers (10 μmol/L), 10μL of TB Green qPCR Master Mix, 2μL of cDNA, and 6.4μL of double-distilled water. The thermal cycling conditions were as follows: initial denaturation at 95 °C for 30s, followed by 40 cycles of denaturation at 95 °C for 15s, annealing at 60 °C for 15s, and extension at 60 °C for 2 min. Fluorescence signals were detected, and relative gene expression levels were calculated using the 2^−ΔΔCT method.

#### EdU incorporation assay

Gastric cancer cells were seeded evenly into confocal dishes, allowed to grow stably, and infected with the recombinant adenovirus. After 24 h, reagent A from the EdU incorporation assay kit was added in the dark, and the cells were incubated for 4–6 h and then fixed with 4% paraformaldehyde at room temperature for 4 h. After fixation, the cells were sequentially washed with PBS, treated with a glycine solution for decolorization, permeabilized with 0.5% Triton X-100, and incubated with the Apollo staining working solution for 30 min. Finally, 1–2 drops of mounting medium containing DAPI were added, and the mixture was evenly applied throughout the confocal dish. The samples were observed and photographed using a confocal laser scanning microscope.

#### Flow cytometry

Gastric cancer cells were seeded evenly in 6-well plates and allowed to grow stably. The cells were subsequently infected with the recombinant adenovirus. After 24 h, the cell suspensions were collected and fixed with 70% ethanol for 4 h. Following fixation, the cells were washed with PBS, incubated in the dark, and stained with propidium iodide (PI) at 37 °C for 30–40 min. Flow cytometry was used to analyze the cell cycle and apoptosis.

#### Transwell assay

Gastric cancer cells were seeded evenly in the upper chambers of Transwell plates containing a matrix membrane and then infected with an appropriate dose of recombinant adenovirus and supplemented with an equal amount of complete culture medium containing 10% serum after 4 h. After 24 h, the cells were allowed to migrate for 5–8 h. The cells were subsequently fixed with 4% paraformaldehyde for 3–4 h at room temperature and stained with crystal violet for 1–3 h until all the cells appeared purple. After washes with PBS, the cells were air-dried in an incubator, and microscopy was performed to observe and acquire images for subsequent analyses.

#### Western blot analysis

Plated gastric cancer cells were washed with PBS, and after the PBS was removed, an appropriate volume of RIPA lysis buffer was added. The cells were lysed on ice for 30 min. Lysates were collected and centrifuged at 12,000×g for 10 min at 4 °C. After centrifugation, the protein concentration in each sample was determined. Following protein quantification, the samples were heated at 99 °C for 10 min to denature the proteins. After denaturation, SDS–PAGE was conducted. The proteins were subsequently transferred to a PVDF membrane. The membrane was blocked with 5% skim milk at 37 °C for 1 h. The PVDF membrane was cut into strips based on the size of the protein bands, and the strips were incubated with the corresponding primary antibodies [anti-GPX4 (ab262509, Abcam, UK), anti-HECTD1-463aa (1:1500), anti-β-actin (1:2500) (ab6276, Abcam, UK), and anti-GAPDH (1:5000) (ab8245, Abcam, UK), anti-SLC7A11 (1:500) (DF12509, Affinity, USA), and anti-FTH1 (1:1000) (DF7705, Affinity, USA)] at 4 °C overnight (12–16 h). After an incubation with the corresponding

species-matched secondary antibodies (1:2500) at room temperature for 50 min, the membranes were exposed.

### LC–MS/MS

Protein samples obtained by enzymatic digestion were subjected to LC–MS/MS analysis to obtain raw mass spectra. The raw files were then analyzed using Byonic software, and the sequences were searched against the UniProt *Homo sapiens* database to identify proteins.

### Co-IP

A total of 5 μg of normal IgG and 5 μg of anti-FLAG antibody were incubated with 50 μL of Protein G Dynabeads. Subsequently, a DSS crosslinker was added to crosslink the Protein G beads with the antibodies. The cross-linked beads were collected after washing to isolate cross-linked normal IgG- and anti-FLAG antibody-bound Protein G beads. These beads were individually incubated with 1 mg of total protein extracted from Hsa_circ_0002301-Flag-overexpressing cells overnight at 4 °C with gentle agitation on a vertical shaker. The following day, magnetic separation was employed to collect the beads. Subsequent washing steps were performed using RIP buffer (1 mL per wash for 5 min each). Finally, 50 μL of SDS loading buffer was added to elute the proteins through an incubation at 95 °C for 5 min. Then, 10 μL aliquots of the aforementioned protein samples were separated on a 10–12% SDS–PAGE gel, and the proteins were subjected to high-resolution silver staining. Differentially migrated protein bands were excised for the mass spectrometry analysis.

### Immunofluorescence staining

MKN45 cells overexpressing Hsa_circ_0002301-Flag were seeded in 24-well plates and detached with trypsin. The resulting single-cell suspensions were seeded into 24-well plates (approximately $5 \times 10^4$ cells per well). After 24 h of incubation, the cells adhered evenly to the plates. The culture medium was discarded, and the cells were washed three times with PBS. The cells were then fixed with 4% paraformaldehyde for 15 min and permeabilized with 2% Triton X-20. Anti-FLAG and anti-GAPDH antibodies were added separately, and the cells were incubated at 4°C overnight. The next day, the cells were washed five times, and the corresponding fluorescent dye-conjugated secondary antibodies were added and incubated at room temperature for 1 h. After the secondary antibodies were discarded, the cells were washed five times. Finally, DAPI was added for staining, and the stained cells were mounted on glass slides to prepare temporary mounts. Images of immunofluorescence staining were acquired using a spinning disk confocal microscope.

### Statistical analysis

All the experiments were conducted in triplicate. The data were analyzed using IBM SPSS Statistics (version 19.0, IBM, USA), and the results are presented as the means ± standard errors of the means (SEMs). The statistical significance of differences was calculated using an unpaired Student's t test. An analysis of disease-free survival (DFS) was conducted using the Kaplan–Meier method and log-rank test. Clinicopathological features were analyzed using the $\chi^2$ test. Cox proportional hazards regression models were used to identify independent prognostic factors associated with DFS. A linear correlation analysis was performed to assess the relationships among hsa_circ_0002301, ferroptosis levels, and tumor size. P values were considered to indicate statistically significant differences.

### Abbreviations

| | |
|---|---|
| ROS | Reactive oxygen species |
| GPX4 | Glutathione peroxidase 4 |
| IRES | Internal ribosome entry site |
| GC | Gastric cancer |
| circRNAs | Circular RNAs |
| MNU | N-methyl-N-nitrosourea |
| PE | Piperazine erastin |
| LC–MS/MS | Liquid chromatography–tandem mass spectrometry |
| HECTD1 | Hect domain E3 ubiquitin protein ligase 1 |
| co-IP | Coimmunoprecipitation |
| Ub | Ubiquitin |
| m6A | N6-methyladenosine |
| MDA | Malondialdehyde |
| GSH | Glutathione |
| GSSG | Oxidized glutathione |
| H&E | Hematoxylin–eosin |
| FNR | Ferroptosis negative regulator |
| miRNA | MicroRNA |
| qRT–PCR | Quantitative polymerase chain reaction |
| GEO | Gene Expression Omnibus |
| RNase R | Ribonuclease R |
| FISH | Fluorescence in situ hybridization |
| OS | Overall survival |
| siRNAs | Small interfering RNAs |
| ORFs | Open reading frames |
| RBPDB | RNA-Binding Protein Database |
| IRES-1 | IRES encompassing nucleotides 4–151 |
| METTL3 | Methyltransferase-like 3 |
| TCGA | The Cancer Genome Atlas |
| GEPIA | Gene expression profiling interactive analysis |
| shRNA | Short hairpin RNA |
| CHX | Cycloheximide |
| RIP | RNA immunoprecipitation |
| RBPs | RNA-binding proteins |
| GO | Gene Ontology |
| FUS | RNA-binding protein FUS |
| ELAVL1 | ELAV-like protein 1 |
| YTHDC1 | YTH domain-containing protein 1 |

## Supplementary Information

The online version contains supplementary material available at https://doi.org/10.1186/s12967-025-06226-7.

Supplementary Material 1

Supplementary Material 2

Supplementary Material 3

Supplementary Material 4

Supplementary Material 5

Supplementary Material 6

Supplementary Material 7

Supplementary Material 8

Supplementary Material 9

Supplementary Material 10

**Acknowledgements**
The authors thank the patients, their families, the investigators, and the staff involved in this study.

**Author contributions**
SW: conceptualization, writing—original draft. CW and JW: conceptualization, supervision, writing—review and editing. FY: writing—review and editing. YH: funding acquisition, software. TC: writing—review and editing. LX: project administration, writing—review and editing. LQ: supervision, writing—review and editing. XW: investigation, resources. YBX, LX and AZ: validation, writing—original draft. LW: resources, formal analysis, and methodology. XH: conceptualization, validation, writing—original draft. All the authors reviewed the manuscript.

**Funding**
This work was supported by the National Natural Science Foundation of China (82372707 and 81902515), the University Natural Science Research Project of Anhui Province (2023AH051771, KJ2021A0857, and 2023AH040254), and the Anhui Provincial Health Commission Provincial Financial Key Projects (AHWJ2023A10126).

**Data availability**
All the data generated or analyzed during this study are included in this published article [and its Supplementary information files]. The raw data supporting the conclusions of this article will be made available by the authors without undue reservation.

## Declarations

**Ethical approval and consent to participate**
With the approval of the Ethics Committee of the First Affiliated Yijishan Hospital of Wannan Medical College, we obtained human gastric cancer tissues and adjacent normal tissues from patients with gastric cancer who were treated at the Department of Gastric Surgery of the First Affiliated Yijishan Hospital of Wannan Medical College. BALB/c-null mice were purchased from the Animal Center of Wannan Medical College (Wuhu, China) and bred under specific pathogen-free conditions. All animal experiments were approved by the Institutional Animal Care and Use Committee of Wannan Medical College.

**Consent for publication**
Not applicable.

**Competing interests**
The authors have no conflicts of interest.

**Author details**
[1]Department of Gastrointestinal Surgery, The First Affiliated Yijishan Hospital of Wannan Medical College, No. 2, Zheshan West Road, Wuhu, Anhui, Anhui 241001, China
[2]Department of Immunology, School of Basic Medical Sciences, Fudan University, Shanghai, China
[3]Anhui Province Key Laboratory of Non-coding RNA Basic and Clinical Transformation, Wuhu, Anhui, China
[4]Department of Ultrasound, Children's Hospital of Nanjing Medical University, Nanjing, Jiangsu, China
[5]Department of Medical Examination Center, The First Affiliated Yijishan Hospital of Wannan Medical College, Wuhu, Anhui, China
[6]Department of Cancer Biology, The University of Texas MD Anderson Cancer Center, Houston, USA
[7]Department of Hepato-Biliary-Pancreatic Surgery, The First Affiliated Hospital of Wannan Medical College (Yijishan Hospital), Wuhu, China

Received: 2 September 2024 / Accepted: 11 February 2025
Published online: 28 February 2025

**References**

1. Al-Mahrouqi H, Parkin L, Sharples K. Incidence of stomach cancer in Oman and the other gulf cooperation council countries. Oman Med J. 2011;26(4):258–62.
2. Jiang F, Shen X. Current prevalence status of gastric cancer and recent studies on the roles of circular RNAs and methods used to investigate circular RNAs. Cell Mol Biol Lett. 2019;24:53.
3. Smyth EC, et al. Gastric cancer. Lancet. 2020;396(10251):635–48.
4. Chen X, et al. Organelle-specific regulation of ferroptosis. Cell Death Differ. 2021;28(10):2843–56.
5. Dixon SJ, et al. Ferroptosis: an iron-dependent form of nonapoptotic cell death. Cell. 2012;149(5):1060–72.
6. Zhang H, et al. Chemotoxicity-induced exosomal lncFERO regulates ferroptosis and stemness in gastric cancer stem cells. Cell Death Dis. 2021;12(12):1116.
7. Ma M, et al. Activation of MAT2A-ACSL3 pathway protects cells from ferroptosis in gastric cancer. Free Radic Biol Med. 2022;181:288–99.
8. Kirtonia A, Sethi G, Garg M. The multifaceted role of reactive oxygen species in tumorigenesis. Cell Mol Life Sci. 2020;77(22):4459–83.
9. Wang Y et al. Iron Metabolism in Cancer. Int J Mol Sci, 2018. 20(1).
10. Stockwell BR, et al. Ferroptosis: a regulated cell death Nexus linking metabolism, Redox Biology, and Disease. Cell. 2017;171(2):273–85.
11. Battaglia AM et al. Ferroptosis Cancer: Mitochondria Meet Iron Maiden Cell Death Cells, 2020. 9(6).
12. Strasser A, Vaux DL. Cell death in the origin and treatment of Cancer. Mol Cell. 2020;78(6):1045–54.
13. Jiang L, et al. Ferroptosis as a p53-mediated activity during tumour suppression. Nature. 2015;520(7545):57–62.
14. Hassannia B, Vandenabeele P, Vanden Berghe T. Targeting ferroptosis to Iron Out Cancer. Cancer Cell. 2019;35(6):830–49.
15. Zhao L, et al. Ferroptosis in cancer and cancer immunotherapy. Cancer Commun (Lond). 2022;42(2):88–116.
16. Lu L, et al. Role of ferroptosis and ferroptosis-related non-coding RNAs in the occurrence and development of gastric cancer. Front Pharmacol. 2022;13:902302.
17. Ou R, et al. Circular RNA circLMO1 suppresses cervical Cancer Growth and Metastasis by triggering miR-4291/ACSL4-Mediated ferroptosis. Front Oncol. 2022;12:858598.
18. Du WW, et al. Identifying and characterizing circRNA-Protein Interaction. Theranostics. 2017;7(17):4183–91.
19. Pamudurti NR, et al. Translation of CircRNAs. Mol Cell. 2017;66(1):9–21..e7.
20. Wu C, et al. Newly discovered mechanisms that mediate tumorigenesis and tumour progression: circRNA-encoded proteins. J Cell Mol Med. 2023;27(12):1609–20.
21. Li F, et al. A peptide CORO1C-47aa encoded by the circular noncoding RNA circ-0000437 functions as a negative regulator in endometrium tumor angiogenesis. J Biol Chem. 2021;297(5):101182.
22. Khan FA, et al. Chimeric Peptides/Proteins encoded by circRNA: an update on mechanisms and functions in human cancers. Front Oncol. 2022;12:781270.
23. Ngo LH, et al. Nuclear export of circular RNA. Nature. 2024;627(8002):212–20.
24. Xu C, et al. A circulating panel of circRNA biomarkers for the noninvasive and early detection of pancreatic ductal adenocarcinoma. Gastroenterology. 2024;166(1):178–e19016.
25. Yang WS, Stockwell BR. Ferroptosis: death by lipid peroxidation. Trends Cell Biol. 2016;26(3):165–76.
26. Shen Z, et al. Emerging strategies of Cancer Therapy based on ferroptosis. Adv Mater. 2018;30(12):e1704007.
27. Jiang X, Stockwell BR, Conrad M. Ferroptosis: mechanisms, biology and role in disease. Nat Rev Mol Cell Biol. 2021;22(4):266–82.
28. Battaglia AM, et al. Iron Administration overcomes resistance to erastin-mediated ferroptosis in Ovarian Cancer cells. Front Oncol. 2022;12:868351.

29. Yang WS, et al. Regulation of ferroptotic cancer cell death by GPX4. Cell. 2014;156(1–2):317–31.
30. Huang D, et al. Tumour circular RNAs elicit anti-tumour immunity by encoding cryptic peptides. Nature. 2024;625(7995):593–602.
31. Deng C, et al. Exosome circATP8A1 induces macrophage M2 polarization by regulating the miR-1-3p/STAT6 axis to promote gastric cancer progression. Mol Cancer. 2024;23(1):49.
32. Wei G, et al. Human gastric cancer progression and stabilization of ATG2B through RNF5 binding facilitated by autophagy-associated CircDHX8. Cell Death Dis. 2024;15(6):410.
33. Chen R, et al. Engineering circular RNA for enhanced protein production. Nat Biotechnol. 2023;41(2):262–72.
34. Xu S, et al. Tumor-tailored ionizable lipid nanoparticles facilitate IL-12 circular RNA delivery for enhanced Lung Cancer Immunotherapy. Adv Mater. 2024;36(29):e2400307.
35. Jin J, et al. A Novel Identified Circular RNA, mmu_mmu_circRNA_0000309, involves in germacrone-mediated improvement of Diabetic Nephropathy through regulating ferroptosis by targeting miR-188-3p/GPX4 Signaling Axis. Antioxid Redox Signal. 2022;36(10–12):740–59.
36. Zhang W, et al. GPX4, ferroptosis, and diseases. Biomed Pharmacother. 2024;174:116512.
37. Li D, et al. CST1 inhibits ferroptosis and promotes gastric cancer metastasis by regulating GPX4 protein stability via OTUB1. Oncogene. 2023;42(2):83–98.
38. Lee S, et al. Autophagy mediates an amplification loop during ferroptosis. Cell Death Dis. 2023;14(7):464.
39. Shi X, et al. Bladder-cancer-derived exosomal circRNA_0013936 promotes suppressive immunity by up-regulating fatty acid transporter protein 2 and down-regulating receptor-interacting protein kinase 3 in PMN-MDSCs. Mol Cancer. 2024;23(1):52.
40. Zhou C, et al. Mutant KRAS-activated circATXN7 fosters tumor immunoescape by sensitizing tumor-specific T cells to activation-induced cell death. Nat Commun. 2024;15(1):499.
41. Pottenger LH, et al. Dose-response and operational thresholds/NOAELs for in vitro mutagenic effects from DNA-reactive mutagens, MMS and MNU. Mutat Res. 2009;678(2):138–47.
42. Morton D, et al. N-Methyl-N-Nitrosourea (MNU): a positive control chemical for p53+/- mouse carcinogenicity studies. Toxicol Pathol. 2008;36(7):926–31.
43. Yang Y, et al. Nedd4 ubiquitylates VDAC2/3 to suppress erastin-induced ferroptosis in melanoma. Nat Commun. 2020;11(1):433.
44. Xu S, et al. The emerging role of ferroptosis in intestinal disease. Cell Death Dis. 2021;12(4):289.
45. Zuo YB, et al. Ferroptosis in Cancer Progression: role of noncoding RNAs. Int J Biol Sci. 2022;18(5):1829–43.
46. Zhang Y, et al. CircDIDO1 inhibits gastric cancer progression by encoding a novel DIDO1-529aa protein and regulating PRDX2 protein stability. Mol Cancer. 2021;20(1):101.
47. Gao X, et al. Circular RNA-encoded oncogenic E-cadherin variant promotes glioblastoma tumorigenicity through activation of EGFR-STAT3 signalling. Nat Cell Biol. 2021;23(3):278–91.
48. Jiang T, et al. A novel protein encoded by circMAPK1 inhibits progression of gastric cancer by suppressing activation of MAPK signaling. Mol Cancer. 2021;20(1):66.
49. Zhu Z, et al. Circular RNA circNHSL1 promotes gastric cancer progression through the miR-1306-3p/SIX1/vimentin axis. Mol Cancer. 2019;18(1):126.
50. Zhang HY, et al. Circular RNA TTBK2 regulates cell proliferation, invasion and ferroptosis via miR-761/ITGB8 axis in glioma. Eur Rev Med Pharmacol Sci. 2020;24(5):2585–600.
51. Sun ZY, et al. circRNADisease v2.0: an updated resource for high-quality experimentally supported circRNA-disease associations. Nucleic Acids Res. 2024;52(D1):D1193–200.
52. Liao S, et al. HECTD1-Mediated ubiquitination and degradation of Rubicon regulates Autophagy and Osteoarthritis Pathogenesis. Arthritis Rheumatol. 2023;75(3):387–400.
53. Duhamel S, et al. The E3 ubiquitin ligase HectD1 suppresses EMT and metastasis by targeting the +TIP ACF7 for degradation. Cell Rep. 2018;22(4):1016–30.
54. Li Y, et al. Overexpression of BIRC6 driven by EGF-JNK-HECTD1 signaling is a potential therapeutic target for triple-negative breast cancer. Mol Ther Nucleic Acids. 2021;26:798–812.
55. Bhardwaj A, et al. Whole proteome analysis of human tankyrase knockout cells reveals targets of tankyrase-mediated degradation. Nat Commun. 2017;8(1):2214.
56. Fang S, et al. circHECTD1 promotes the silica-induced pulmonary endothelial-mesenchymal transition via HECTD1. Cell Death Dis. 2018;9(3):396.
57. Pradhan A, et al. Novel FOXF1-Stabilizing compound TanFe stimulates Lung Angiogenesis in Alveolar Capillary Dysplasia. Am J Respir Crit Care Med. 2023;207(8):1042–54.


## Publisher's note